LETTERS

Differentiation of the asteroid Ceres as revealed by its shape

P. C. Thomas[1], J. Wm. Parker[2], L. A. McFadden[3], C. T. Russell[4], S. A. Stern[2], M. V. Sykes[5] & E. F. Young[2]

The accretion of bodies in the asteroid belt was halted nearly 4.6 billion years ago by the gravitational influence of the newly formed giant planet Jupiter. The asteroid belt therefore preserves a record of both this earliest epoch of Solar System formation and variation of conditions within the solar nebula. Spectral features in reflected sunlight indicate that some asteroids have experienced sufficient thermal evolution to differentiate into layered structures[1]. The second most massive asteroid—4 Vesta—has differentiated to a crust, mantle and core[2,3]. 1 Ceres, the largest and most massive asteroid, has in contrast been presumed to be homogeneous, in part because of its low density, low albedo and relatively featureless visible reflectance spectrum, similar to carbonaceous meteorites that have suffered minimal thermal processing[4]. Here we show that Ceres has a shape and smoothness indicative of a gravitationally relaxed object. Its shape is significantly less flattened than that expected for a homogeneous object, but is consistent with a central mass concentration indicative of differentiation. Possible interior configurations include water-ice-rich mantles over a rocky core.

We obtained Hubble Space Telescope (HST) observations during nine orbits in December 2003 and January 2004 using the High Resolution Channel (HRC) of the Advanced Camera for Surveys (ACS)[5]. Six consecutive HST orbits were used to provide full coverage of Ceres' 9.075-h rotation period (Fig. 1), and three additional orbits separated by 120° in rotational phase were used to obtain higher spatial resolution by making small offsets (dithering) of the telescope between exposures. The data were processed through the standard HST pipeline, followed by processing with software using standard HRC functions to remove geometric distortion.

Limb profiles were measured for 217 images using techniques that locate sharp contrast boundaries to ~0.1 pixel (ref. 6). We find that the shape of Ceres is rotationally symmetric to the limit of measurement accuracy (Fig. 2a, b), and is well described by an oblate spheroid of axes $a = 487.3 \pm 1.8$ km and $b = 454.7 \pm 1.6$ km (1σ). Individual limb profiles are well fitted by ellipses: combining data for all 217 limbs, the root mean square radial error is 0.16 pixels, or ~4.8 km (Fig. 2c).

Because the equatorial axes are the same within <2 km, and mean residuals to ellipses fitted to the limbs are <5 km, we conclude that Ceres is a relaxed object; that is, its shape is determined by hydrostatic equilibrium. A globally relaxed object can still have topography, such as craters, because relaxation timescales are inversely proportional to the wavelength of the topography[7]. The limb topography from our data are smoothed over the 30-km pixel size, and we would probably not detect topography <60 km across. Occultation data[8], which effectively sample at points, have average residuals of about 5 km, with maximum topography about 10 km. Such relief is consistent with our data.

If water ice is important in the rheology of Ceres' near-surface region, relief in large impact basins on icy satellites is our best practical guide to how much relief there should be on Ceres. Because larger craters are relatively more shallow than small ones, even craters over 200 km across have depths of less than 10 km (ref. 9). As an example, there are excellent limb profile data on the 400-km crater Odysseus on Saturn's moon Tethys (mean radius of 535 km) that show maximum relief of about 8 km (ref. 9); smoothed to 30 km spacing, this would show ~5 km relief. Such relief on Ceres is difficult to detect by current means, and might be reduced by the slightly higher expected temperatures compared to Tethys. Thus, if ice is involved in the rheology of Ceres, it could retain a substantial crater record without affecting the basic relaxed shape. For comparison, Vesta, which is clearly a differentiated object with a basaltic crust, does not fit an equilibrium form[10,11], either in the match of overall dimensions to an equilibrium form (10 km variations), or in the limb topography (up to 20 km of relief[10]). Given the similar gravity on the two objects (~ 25 cm s^{-2}), the difference in shapes probably reflects
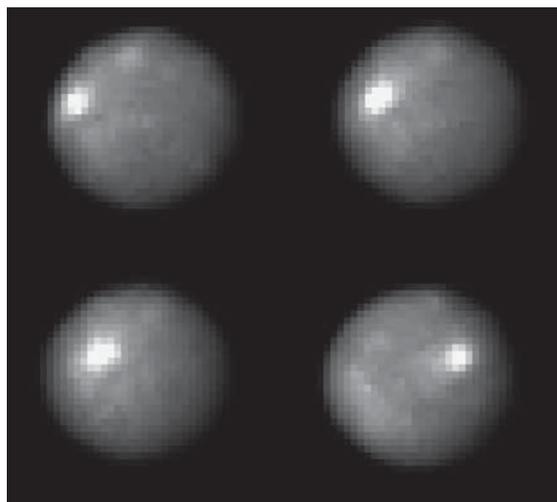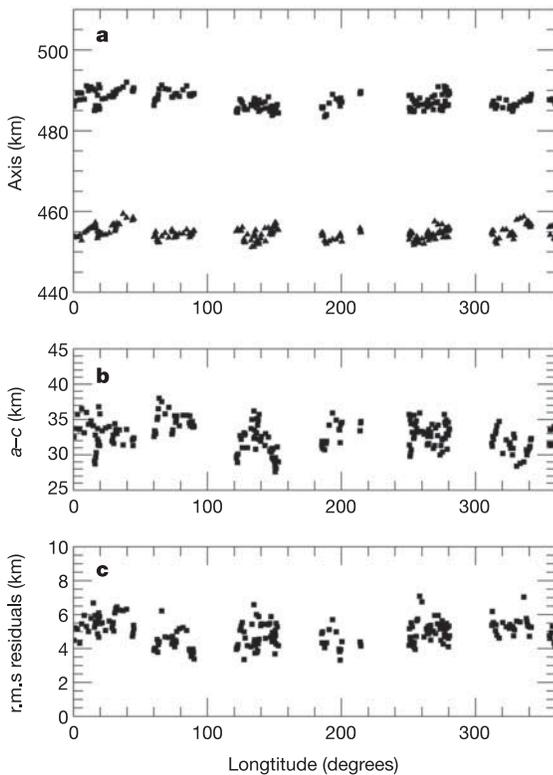

Figure 1 | Rotation of a bright spot on Ceres. Advanced Camera for Surveys (ACS) images of Ceres, showing rotation of a bright spot. The images are strongly contrast-enhanced to emphasize the feature; actual contrasts on the surface are only a few percent. The illuminated limb is the left side, centred 17° up from horizontal. The limb ellipse fits, combined with tracking of the bright spot visible in 51 images covering 93° of rotation, allow us to find a spin vector of right ascension (RA) 291° and declination (dec.) 59°. The uncertainty ~5° clarifies ambiguities among previous measurements[28,29]. This spin pole means that Ceres has an obliquity of only ~3°, which is consistent with previous interpretation, but reduces the uncertainty.

[1]Center for Radiophysics and Space Research, Cornell University, Ithaca, New York 14853, USA. [2]Department of Space Studies, SwRI, 1050 Walnut Street, Boulder, Colorado 80302, USA. [3]Department of Astronomy, University of Maryland, College Park, Maryland 20742, USA. [4]IGPP & ESS, University of California Los Angeles, Los Angeles, California 90095, USA. [5]Planetary Science Institute, 1700 East Fort Lowell, Tucson, Arizona 85719-2395, USA.

different rheologies, with Ceres unable to sustain as much topography as Vesta. Smaller asteroids for which there are good shape data are irregular in form, and expectations of equilibrium forms among many asteroids have not been met[12]. Thus, Ceres is as yet the only known relaxed asteroid.

The difference between the long and short axes of an equilibrium spheroid is directly proportional to the square of the rotation rate, is inversely proportional to the mean density[13,14], and is affected by the distribution of mass. Thus, the shape may be used to investigate global internal properties. Based on the maximum and minimum values of recent measurements of Ceres' mass of $(9.47 \pm 0.05) \times 10^{20}$ kg and $(9.35 \pm 0.08) \times 10^{20}$ kg (refs 11, 15), we use an average mass of $(9.395 \pm 0.125) \times 10^{20}$ kg. With our mean radius of 476.2 ± 1.7 km (1σ, calculated from each observed long and short axis), this mass corresponds to a density of $2,077 \pm 36$ kg m^{-3}. This density falls within the range of bulk densities for Murchison-like (CM) carbonaceous chondrites[16], but is larger than the density of $1,300$ kg m^{-3} of the C-type asteroid Mathilde[17], whose low density is attributed to interior voids. Porosity is not expected to be globally important for Ceres, as the central pressure of a body such as Mathilde is reached within ~300 m of the surface of Ceres.

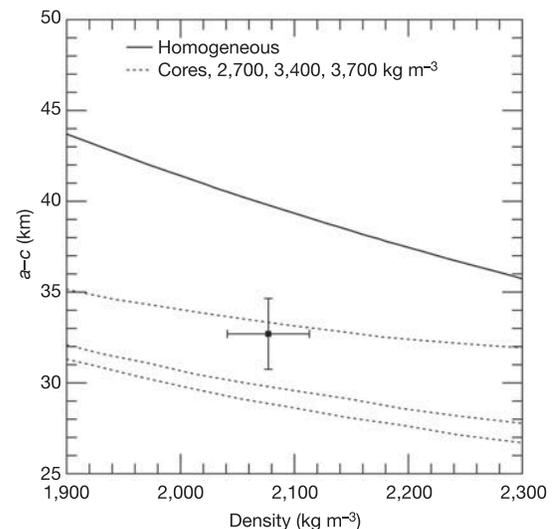For a mean density of $2,077$ kg m^{-3}, the equilibrium shape $(a - c)$ would be 39.7 km (ref. 14). Our value of $a - c$ of 32.6 ± 1.95 km (1σ) differs from this value by more than 3σ. Thus, the observed flattening is inconsistent with that expected for a homogenous body[14]. The same test was previously applied to the occultation data[8] but used a higher mass, and thus obtained a result consistent with a homogeneous Ceres. However, we must evaluate the possible systematic errors to determine how relevant the formal uncertainties are.

The primary contributor of error in the shape is any difference in systematic errors in detecting the limb along the long and short axes. Consistent errors in the same sense will not affect the shape solution, only the mean radius. We estimate possible systematic errors in the measurement of the long and short axes by comparison to past experience[6] with the limb-finding routine on sections of limbs that include greatly different albedos and different scattering functions. Large photometric variations cause systematic changes of individual limb coordinates of almost always less than 0.3 pixels. If entirely concentrated on one axis, this error would change the fitted semi-axis by 0.15 pixels. Given that the photometric variation around the disk of Ceres is small, and is not restricted to one projected axis, an assumption of maximum possible errors in $a - c$ of 0.15 pixels, or 4.5 km, is appropriately conservative, and can be regarded as a 3σ error.

The best check of the absolute dimensions of Ceres comes from stellar occultation measurements[8]. This work gave axes of 479.6 ± 2.4 by 454.3 ± 4.5 km if minimizing radial residuals, and 481.6 ± 2.4 by 450.1 ± 2.0 km (1σ values) if minimizing the timing errors. The two solutions give $a - c$ values, 25.3 and 31.5 km, that are less than our value of 32.6 km. The occultation observed only one cross-section of Ceres, but because the HST data show that the long axis varies by only a few kilometres around the body, the comparison

Figure 2 | **The shape of Ceres. a,** Short (polar) and long (equatorial) projected axes of Ceres plotted versus an arbitrary reference viewing longitude. The pixel scale of 0.025 arcsec in the geometrically corrected images is about 30 km per pixel at the geocentric distance of Ceres (~1.65 AU) during the observations. The low solar phase angles of 5.4°–7.5° allow use of both the limb and terminator positions, but induce radius errors between the terminator and ideal body outline. Terminator portions of raw profiles were corrected for predicted position dependent upon solar phase and azimuth in the image. These corrections result in changes to fit radii of 1–2 km, which are ~0.03–0.06 pixels. The sub-observer latitudes on Ceres were −0.4° to +2.1° N. This equatorial viewing geometry means the projected axes are essentially identical to the actual shape. Three filter bands were used, centred at 535, 335 and 223 nm (ref. 30); averaged by filter, the fit axes differ by less than 1 km. **b,** Difference between long (*a*) and short (*c*) axes of Ceres as a function of arbitrary observer longitude. **c,** Smoothness of limb of Ceres. Root mean square residuals of fits to ellipses are shown as a function of observer longitude.

Figure 3 | **Interior models of Ceres.** Shape and density of Ceres compared to Maclaurin spheroids. Shape is given as the difference between the equatorial, *a*, and polar, *c*, radii. Solid curve is the expected shape as a function of density for a relaxed homogeneous body with a rotation period of 9.075 h. Plotted point is the average density of Ceres and the observed shape. Uncertainty in the shape value is the standard deviation (1σ) of all measures of $a - c$. Occultation data[8] suggest that $a - c$ may be less than our nominal value. Uncertainty in the density is the root sum square of the fractional mass and volume uncertainties. Dashed lines give the equilibrium shape for a simple core/mantle model of rock and water ice: core densities are 2,700, 3,400 and 3,700 kg m^{-3}, going from upper to lower dashed curves. For a homogeneous object the size of Ceres, the numerical determination of shape $a - c$ is within 150 m of the theoretical value[14], indicating the level to which the model predicted shapes are accurate.

is meaningful and shows a mean radius within 6 km of our value.

An $a - c$ value smaller than that expected of a homogeneous object indicates mass concentration towards the centre[13]. We would expect a body of the size and solar distance of Ceres to be composed principally of rock and water ice[4]. However, the mineralogy and density of a non-ice component is not well constrained, and may itself depend upon thermal history[2,4]. To construct a simple interior model, we assume a range of core densities: one appropriate for the grain density of primitive carbonaceous materials ($2,700 \, \text{kg m}^{-3}$), and one that spans recent density measurements of Vesta[11,15], 3,400 to $3,700 \, \text{kg m}^{-3}$. For a particular mean density, and assuming a water-ice mantle, a choice of the core density establishes the relative core volume, and the equilibrium shape is determined by numerical methods[18] where gravitational potential is equal over the surface. A rocky core and a water-ice mantle give a shape consistent with our observations (Fig. 3). Assuming the densest core materials and the nominal mean density of $2,077 \, \text{kg m}^{-3}$, ice mantles are 110–124 km thick and constitute 24–26% of the body mass. The lighter core material requires a mantle thickness of 66 km and a 16% ice mass. Even the minimum mantle thickness is greater than the likely excavation depths of craters a few hundred kilometres across[19].

An alternative interpretation of the shape would be that Ceres is homogeneous and that its shape stabilized at a longer spin period, ~9.93 h, and has not relaxed after subsequent spin-up to its present period of 9.075 h. Tidal interactions with other asteroids are incapable of this spin-up, and impacts large enough to impart the necessary angular momentum would leave obvious topography[20], given an assumption that the shape is 'frozen.'

A water fraction of ~25% is reasonable for objects at this solar distance[21,22]. However, predictions of how much water ends up in a frozen ice mantle, an ocean, or hydrated silicate minerals are very model dependent[3]. In any case, the surface of Ceres is dark and devoid of spectral signatures of water ice, though bound water and ammoniated silicates may be present[23–25]. Near-infrared observations of Ceres indicate evidence of some aqueous alteration, at a temperature not exceeding 400 °C (ref. 26). The relaxed state, differentiated structure, and the mean density strongly suggest water ice as the primary mantle constituent. The difference between Ceres' surface and those of icy satellites of Jupiter and Saturn is not surprising, given the much higher heating available at Ceres' distance from the Sun, which makes water ice unstable at the surface[27]. If water ice has been at the surface of Ceres, it may currently be hidden just below a thin residual layer of clay and dark carbonaceous materials. Our findings indicate that the Dawn mission, which will orbit Ceres in 2015, will find a globally relaxed and differentiated object, but which should retain a visible cratering record, and possibly tectonic features similar to those on some icy satellites.

1. McSween, H. Y., Ghosh, A., Grimm, E., Wilson, L. & Young, E. D. in *Asteroids III* (eds Bottke, W. *et al.*) 559–571 (Univ. Arizona Press, Tucson, 2002).
2. McCord, T. B., Adams, J. B. & Johnson, T. V. Asteroid Vesta: Spectral reflectivity and compositional implications. *Science* 168, 1445–1447 (1970).
3. Ghosh, A. & McSween, H. Y. Jr A thermal model for the differentiation of asteroid 4 Vesta, based on radiogenic heating. *Icarus* 134, 187–206 (1998).
4. McCord, T. B. & Sotin, C. Ceres: Evolution and current state. *J. Geophys. Res.* 110, E05009, doi:10.1029/2004JE002244 (2005).
5. Parker, J. Wm. *et al.* Ceres: High-resolution imaging with HST and the determination of physical properties. *Adv. Space Res.* (in the press).
6. Thomas, P. C. *et al.* The shape of Io from Galileo limb measurements. *Icarus* 135, 175–180 (1998).
7. Johnson, T. V. & McGetchin, T. R. Topography on satellite surfaces and the shape of asteroids. *Icarus* 18, 612–620 (1973).
8. Millis, R. L. *et al.* The size, shape, density, and albedo of Ceres from its occultation of BD + 8°471. *Icarus* 72, 507–518 (1987).
9. Schenk, P. M. Crater formation and modification on the icy satellites of Uranus and Saturn—Depth/diameter and central peak occurrence. *J. Geophys. Res.* 94, 3813–3832 (1989).
10. Thomas, P. C. *et al.* Impact excavation on asteroid 4 Vesta: Hubble Space Telescope results. *Science* 277, 1492–1495 (1997).
11. Viateau, B. & Rapport, N. Mass and density of asteroids (4) Vesta and (11) Parthenope. *Astron. Astrophys.* 370, 602–609 (2001).
12. Hestroffer, D. On equilibrium shapes among binary asteroids. *Bull. Am. Astron. Soc.* 36, 861 (2004).
13. Dermott, S. F. Shapes and gravitational moments of satellites and asteroids. *Icarus* 37, 575–586 (1979).
14. Chandrasekhar, S. *Ellipsoidal Figures of Equilibrium* (Yale Univ. Press, New Haven, 1969).
15. Michalak, G. Determination of asteroid masses—I. (1) Ceres, (2) Pallas and (4) Vesta. *Astron. Astrophys.* 360, 363–374 (2000).
16. Britt, D. T. & Consolmagno, G. J. Stony meteorite porosities and densities: A review of the data through 2001. *Meteorit. Planet. Sci.* 38, 1161–1180 (2003).
17. Veverka, J. *et al.* NEAR's flyby of 253 Mathilde: Images of a C asteroid. *Science* 278, 2109–2112 (1997).
18. Thomas, P. C. Gravity, tides, and topography on small satellites and asteroids—Application to surface features of the Martian satellites. *Icarus* 105, 326–344 (1993).
19. Melosh, H. J. *Impact Cratering: A Geologic Process* (Oxford Univ. Press, New York, 1989).
20. Farinella, P., Davis, D. R., Paolicchi, P., Cellino, A. & Zappala, Z. Asteroid collisional evolution: An integrated model for the evolution of asteroid rotation rates. *Astron. Astrophys.* 253, 604–614 (1992).
21. Wilson, L., Keil, K., Browning, L. B., Krot, A. N. & Bourcher, W. Early aqueous alteration, explosive disruption, and re-processing of asteroids. *Meteorit. Planet. Sci* 34, 541–557 (1999).
22. Grimm, R. E. & McSween, H. Y. Water and the thermal evolution of carbonaceous chondrite parent bodies. *Icarus* 82, 244–280 (1989).
23. Lebofsky, L. A. *et al.* The 1.7- to 4.2-micron spectrum of asteroid 1 Ceres—Evidence for structural water in clay minerals. *Icarus* 48, 453–459 (1981).
24. Feierberg, M. A., Lebofsky, L. A. & Larson, H. P. Spectroscopic evidence for aqueous alteration products on the surfaces of low-albedo asteroids. *Geochim. Cosmochim. Acta* 45, 971–981 (1981).
25. King, T. V. *et al.* Evidence for ammonium-bearing minerals on Ceres. *Science* 255, 1551–1553 (1992).
26. Rivkin, A. S. *Observations of Main-belt Asteroids in the 3-μm Region.* Ph.D. dissertation, Univ. Arizona (1997).
27. Fanale, F. P. & Salvail, J. R. The water regime of asteroid 1 Ceres. *Icarus* 82, 97–110 (1989).
28. Saint-Pe, O., Combes, M. & Rigaut, F. Ceres surface properties by high-resolution imaging from earth. *Icarus* 105, 263–271 (1993).
29. Drummond, J. O., Fungate, R. Q. & Christou, J. G. Full adaptive optics images of asteroids Ceres and Vesta; rotational poles and triaxial ellipsoid dimensions. *Icarus* 132, 80–99 (1998).
30. Pavlovsky, C. *et al.* ACS Instrument Handbook, Version 5.0 (Space Telescope Science Institute, Baltimore, 2004).